CrystEngComm

Accepted Manuscript

This article can be cited before page numbers have been issued, to do this please use: C. Guo, Y. zhang, L. Zhang, Y. Zhang and J. Wang, *CrystEngComm*, 2018, DOI: 10.1039/C8CE00954F.

ROYAL SOCIETY OF CHEMISTRY

rsc.li/crystengcomm

View Article Online
DOI: 10.1039/C8CE00954F

Journal Name

COMMUNICATION

2-Methylimidazole-Assisted Synthesis of Two-Dimensional MOF-5 Catalyst with Enhanced Catalytic Activity for the Knoevenagel Condensation Reaction

Received 00th January 20xx,
Accepted 00th January 20xx

DOI: 10.1039/x0xx00000x

www.rsc.org/

Changyan Guo [a], Yonghong Zhang*[a], Li Zhang [a], Yi Zhang [b], Jide Wang*[a]

We report a facile strategy to fabricate two-dimensional (2D) MOF-5 with a thickness of 4 nm by 2-methylimidazole (2-MI) as a coordination regulator. 2-MI can inhibit the growth of MOF-5 in the vertical direction by competitive coordination to obtained 2D MOF-5. A series of test results revealed that 2-MI can present in the crystal structure of MOF-5 nanosheets by coordination or adsorption. In addition, more exposed catalytically active sites and the presence of weak basic sites (-NH) in MOF-5 nanosheets is benefit to enhance its catalytic performance in the Knoevenagel condensation.

Two-dimensional (2D) materials have attracted much research interest due to their unique two-dimensional (2D) geometry, nanoscale thickness and high surface-area-to-volume ratio, as well as their diverse applications such as in electrocatalysis,[1] chemical gas sensor,[2] energy storage,[3] and biomedical techniques.[4] As a promising branch of 2D materials, 2D metal-organic framework (MOF) nanosheets perform better than traditional bulk MOF materials.[5] On the one hand, the ultra-thin nanosheets are favoured in gas molecule transport, revealing the potential of MOFs in gas storage.[6] On the other hand, a large number of active sites are exposed on the surface of the 2D MOF nanosheets, and consequently increasing their performance in catalysis,[5b,5c] separation,[7] and sensing.[8] Compared with the extensive application of bulk MOF in catalysis,[9] however, to the best of our knowledge, applications of 2D MOFs in catalytic oganic reactions are rare.[1,5b,5c] Therefore, the design and synthesis of 2D sheet MOFs materials have been of particular importance since it not only can improve the performance of existing MOF materials, but also can be extended to develop novel materials with proposed functions.

Common methods for synthesizing 2D MOF nanosheets include sonication exfoliation,[10] interfacial syntheses,[5b,11] three-layer syntheses,[7] templated syntheses[12] and surfactant-assisted syntheses.[13] Exfoliation is the most preferred method for the preparation of 2D MOF nanosheets, which usually need to break the weak interlaminar forces caused by hydrogen bonds or van der Waals forces, etc. For other methods, however, some special reagents or treatments are usually needed to control the growth rates of MOF materials in the third direction (Z) for obtaining nanosheets.[5a] Despite all the recent achievements in the synthesis of 2D MOF nanosheets used as a catalyst,[14] there remains great challenges to develop new surfactants or assistance compounds, which not only can regulate the morphology of MOFs, but also can act as a catalyst to improve its catalytic performance.[5a]

MOF-5 is a typical MOFs prepared by Yaghi and co-workers.[15] It is built from $[Zn_4O]^{6+}$ clusters and H_2BDC ligands forming a porous cubic framework.[16] This unique structure gives MOF-5 remarkably large pore volume, large surface area, and relatively high thermal stability.[17] Although MOF-5 exhibits considerable potential applications in many fields,[18] it has few applications in catalytic organic reactions, due to its large crystal size and weak base catalytic sites. Rational design and synthesis of the MOF-5 catalyst with more active sites will greatly expand the application prospects of MOF-5 in catalysis. In our previous research,[19] we serendipitously found that the 2-MI is an efficient modulator for tuning crystal morphology and size of Co-MOF-74, and the MOFs regulated by 2-MI exhibit enhanced catalytic activity for oxidizing of benzylic C–H bonds.

In continuation of our efforts to develop efficient and reusable heterogeneous for green synthetic methods,[19,20] herein, a 2D MOF-5 catalyst with enhanced catalytic activity was synthesized by addition of 2-MI as a coordination modulator and Lewis basic site. The mechanism of 2-MI affecting the crystallization process during the growth of MOF-5 crystals has been elucidated, and these MOF nanosheets have excellent catalytic activity in the Knoevenagel condensation reaction. We believe that this approach toward the size/morphology-controlled synthesis of 2D catalysts, and the reveal of the formation mechanism will be helpful for controlling morphologies of MOFs and improving their catalytic properties.

The 2D MOF-5 nanosheets catalyst was synthesized by using the 2-MI-assisted synthetic method. For 2-MI, the lone pair on the nitrogen atom is easy to compete with that of H_2BDC linker

[a] Key Laboratory of Oil and Gas Fine Chemicals, Ministry of Education & Xinjiang Uygur Autonomous Region, College of Chemistry and Chemical Engineering of Xinjiang University, Urumqi 830046, P. R. China. E-mail: zhzhzyh@126.com; awangjd@sina.cn.
[b] Key Laboratory of Resources Chemistry of Nonferrous Metals (Ministry of Education), College of Chemistry and Chemical Engineering, Central South University, Changsha, 410083, P. R. China.

View Article Online
DOI: 10.1039/C8CE00954F

for the coordination of the metal ions. 2-MI can also acts as a base for the deprotonation of thecarboxylic acid ligands. Thus, it will affect crystal nucleation and growth by both competitive coordination and deprotonation equilibria. Furthermore, the 2-MI can be selectively attached to the surface of the MOFs, which stabilizes the MOF-5 nanosheets and restricts their growth along the vertical direction,[5a,21] leading to the formation of ultrathin MOF-5 nanosheets (Fig. 1).

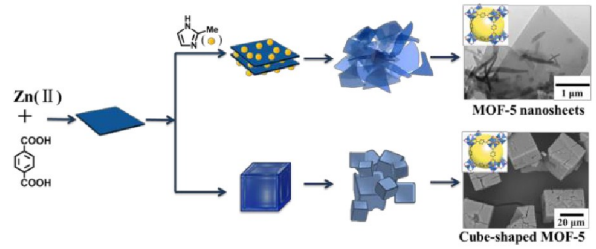

Fig. 1 Simplified figure illustrates the synthesis process of MOF-5 nanosheets.

In MOF-5, the slowest growing directions are along the ⟨100⟩ zone axes, affording cubic morphology.[22] SEM (Fig. 2a, b) and TEM (Fig. 2c) analysis revealed that 2-MI had a pronounced influence on the morphology of MOF-5. In the absence of 2-MI, the MOF-5 crystals had a cubic morphology with a diameter of approximately 40 μm, which was identical to those synthesized by using a classical solvothermal method.[23] In the presence of 4 mM 2-MI, MOF-5 nanosheets were obtained (Fig. S1). The TEM measurements also reveal that the samples exhibit flaky layered morphologies with a smooth surface. PXRD (Fig. 2d) of the MOF-5 nanosheets obtained with 2-MI fully matches with the MOF-5 pattern and the theoretical simulation spectrum derived from single-crystal structure data,[15] indicating that the MOFs structure was not affected by 2-MI. The infrared (IR) spectroscopy results further confirmed the crystal structure of MOF-5 catalyst almost retained its inherent nature after treated with 2-MI (Fig. 2e). The selected area electron diffraction (SAED) pattern showed that the as-synthesized MOF-5 is polycrystalline (Fig. 2f). It gives well-defined reflections corresponding to the [100] zone axis orientation of MOF-5, further confirming the crystal structure.[22c]

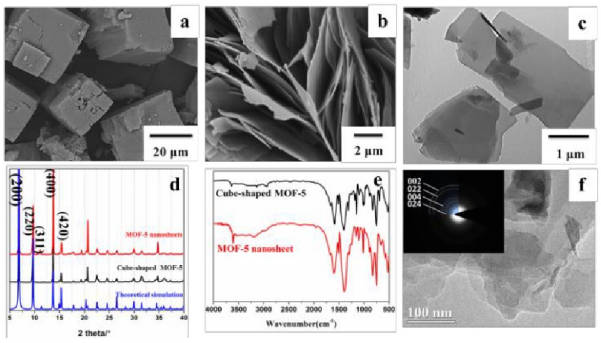

Fig. 2 a) SEM of cubic MOF-5; b) SEM of MOF-5 nanosheets; c) TEM of MOF-5 nanosheets; d) PXRD of MOF-5 nanosheets and theoretical simulation; e) IR of MOF-5 nanosheets and cubic MOF-5; f) TEM graphs and SAED patterns of MOF-5 nanosheets.

Atomic force microscopy (AFM) was conducted to determine the thickness of the MOF-5 nanosheets. The height difference between an H_2BDC unit and a surface Zn^{2+} ion is 0.85 nm.[22b] The full monolayer possesses a height of 1.3 nm revealed by Attfield and co-works,[22b] which is equivalent to the d_{200} crystal spacing (1.28 nm). The measured height at the highest point of the nucleus is around 4 nm (Fig. 3), indicating a pile of three monolayers.

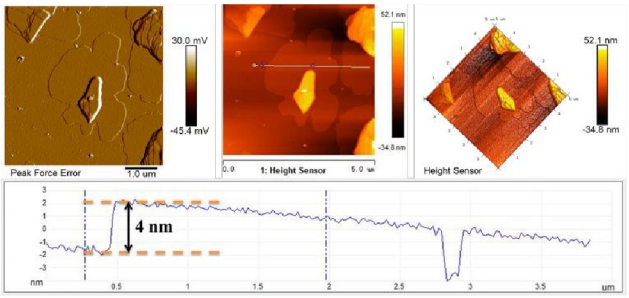

Fig. 3 AFM topography and corresponding height profile images of 2D MOF-5 nanosheets.

According to relevant reports[21,22] and our results, a plausible crystal growth mechanism of MOF-5 is proposed (Fig. 4). The framework of MOF-5 was established by a process of nucleation and spreading of different sub-layers of nanoplatelets. These nanoplatelets aggregated with the connection of H_2BDC molecules to form microplates, which further loosely gathered together to form a cubic MOF-5 crystal with the assistance of H_2BDC. The addition of 2-MI into the growth solutions affected the morphology in crystals by rapid deprotonation and competitive intercalation increasing the nucleation rate. At the first stage of the formation of $Zn_5(OH)_8(NO_3)_2 \bullet 2H_2O$ nanoplatelets, H_2BDC ions inserted into the nanoplatelets via anion exchange. With the NO_3^- anions fully replaced by H_2BDC ions, a phase transformation would occur to form MOF-5 nanoplatelets. If no 2-MI presented in the environment of crystal growth, the resulting MOF-5 nanoplatelets would accumulate with the connection of H_2BDC molecules until large cubic crystals were formed. However, by introducing 2-MI into the crystal growth system, single coordinate 2-MI could compete with H_2BDC and coordinate with Zn^{2+} on the surface of MOF-5 nanoplatelets, which prevented further linking of nanoplatelets and restricted their growth along the vertical direction, leading to the formation of ultrathin MOF-5 nanosheets.

To confirm the existence of 2-MI molecules in the crystal structure, Thermogravimetric Analysis (TGA) and Energy-Dispersive X-Ray Spectroscopy (EDS) elemental mapping, X-ray Photoelectron Spectroscopy (XPS), N_2 adsorption/desorption isotherms and Temperature Programmed Desorption (NH_3-TPD and CO_2-TPD) were performed. The EDS (Figure 5a, b) results confirm that the corresponding metal elements are evenly distributed on the whole surface. Importantly, the content of nitrogen on the surface of exposed facets is more than on cubic MOF-5, proving the 2-MI being present on the surface of the MOF-5 nanoplatelets. TGA results show that MOF-5 nanosheet has similar thermal stabilities compared with cubic MOF-5, and the crystal structure decomposes at higher than 400 °C (Figure 5c). The first weight loss stage is attributed to the release of physically adsorbed solvent

View Article Online
DOI: 10.1039/C8CE00954F

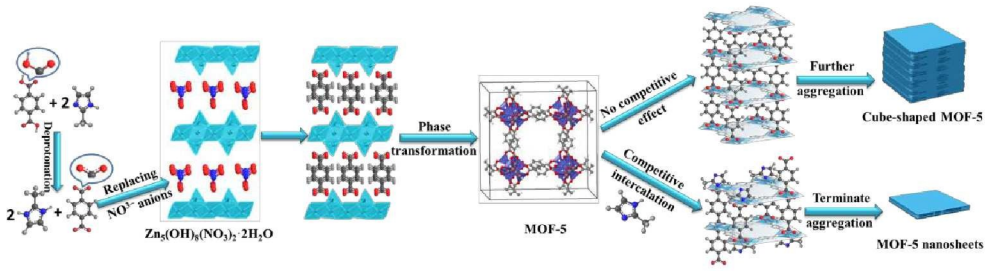

Fig. 4 Schematic drawing of a proposed formation mechanism of MOF-5 nanosheets by regulation of 2-MI.

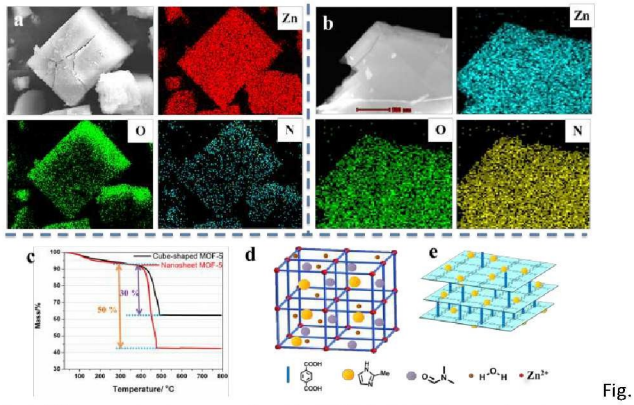

Fig. 5 a) EDS mapping images of cubic MOF-5; b) EDS mapping images of MOF-5 nanosheets; c) TGA images of MOF-5 nanosheets; d) The 2-MI absorbed within the pores of the MOF-5 nanosheets; e) The 2-MI attached to the surface of the MOF-5 nanosheets.

molecules in the MOF framework (such as H_2O and EtOH). The second stage, ranging from 300 to 400 °C, is due to the further release of DMF absorbed within the pores or on the surface of the unreacted ligands. The third weight loss stage at temperatures higher than 400 °C comes from the decomposition of the crystal structure.[21] Notably, the third weight loss of cubic MOF-5 is about 30% corresponding to the decomposition of H_2BDC, resulting in the final composition of ZnO. While the third weight loss of MOF-5 nanosheets increases to 50%, which further confirms the existence of 2-MI molecules in the crystal structure of MOF-5 nanosheets (Figure 5d, e), which is consistent with the hypothesis that the 2-MI coordinates with the Zn^{2+} to prevent further aggregation of nanoplatelets. The XPS results indicated that there is no peak of N 1s was observed in cubic MOF-5, while a distinct N 1s peak appeared in the MOF-5 nanosheets due to the existence of 2-MI (Fig. 6). The N_2 adsorption/desorption isotherms of the 2D MOF-5 were characterized at 77 K (Fig. S2). The 2D MOF-5 exhibited a lower specific surface areas of 550 $m^2 \bullet g^{-1}$ (Table S1), which may be due to the fact that 2-MI occupies the pore of MOF-5 nanosheets. In addition, NH_3-TPD and CO_2-TPD (Fig. S3) were performed on cubic MOF-5 and MOF-5 nanosheets to compute the number and strength of acidic and basic sites. Form the CO_2-TPD result of MOF-5 nanosheeets can been seen, a weak site located at 193 °C appears in the spectra of MOF-5 nanosheets, and a moderate acid site also appears at 270 °C, which make the MOF-5 nanosheets has distinctively higher concentration of weak basic sites. This indicates the presence of uncoordinated 2-MI molecules in MOF-5 nanosheets, which is beneficial for base catalyzed reactions. All above results confirmed that 2-MI exists in the crystal structure of MOF-5 nanosheets in two forms: one is directly present in the surface or pore of the nanosheet just as a guest molecule (Figure 5d); the second is present in the crystal structure of MOF-5 via coordination with the metal (Figure 5e).

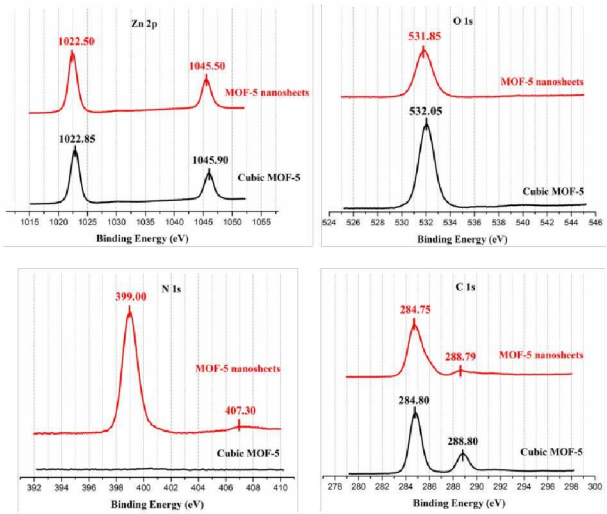

Fig. 6 XPS Zn 2p, C 1s, N 1s and O 1s spectra of the cubic MOF-5 and MOF-5 nanosheets.

Furthermore, we have been systematically studied the catalytic properties of MOF-5 nanosheets for the Knoevenagel condensation reaction of aldehyde and malononitrile (Scheme 1), which is mainly catalyzed by MOFs with Lewis basic sites in heterogeneous catalysis.[24] In this situation, catalysts (such as amide functionalized MOFs) with adequate acid-base pairs are more active than fully acidic/basic catalysts.[25] Our newly synthesized MOF-5 nanosheets have both Lewis acidic sites (Zn^{2+}) and basic sites (2-MI). Therefore, the nanosheets possibly can serve as a catalyst for the Knoevenagel condensation reaction (Scheme 1). Before the catalytic reaction, MOF-5 nanosheets were soaked in methanol for five days to exchange the guest molecules. Evaluation of the catalytic abilities was performed at room temperature under solvent-free condition by comparing different groups (Fig. S4). It was found the Knoevenagel condensation did not process in the absence of a catalyst, and the combination of 2-MI/H_2BDC/zinc salts only afforded 37% yield of 2-benzylidenemalononitrile. These indicated that the active sites

View Article Online
DOI: 10.1039/C8CE00954F

coordinated in MOF have superior catalytic activity. The mixture of 2-MI with cubic MOF-5 although can effectively improve the catalytic performance of cubic MOF-5, this combination still showed a lower catalytic efficiency compared with 2D MOF-5 catalyst, and its cyclic utilization was difficult to achieve. On the contrary, the as-synthesized MOF-5 nanosheets catalyst can be recycled at least for five times without a significant degradation in catalytic activity (Fig. S5). XRD result of the reused catalyst implied that the MOF-5 nanosheets well maintains the crystal structure of MOF-5 during recycling, showing good stability (Fig. S6). The superior catalytic performance of 2D MOF-5 can be attributed to the following three aspects: Firstly, the formation of nanosheets can expose more catalytically active sites; secondly, the presence of crystal defects in the nanosheets is beneficial to the contact of the reaction substrate with catalytically active sites; finally, the uncoordinated 2-MI in the crystal structure can act as a base catalytic site to enhance the catalytic performance of MOF-5 nanosheets.

In order to further demonstrate the applicability of the current 2D MOF-5 catalyst, gram-scale experiments were carried out under modified reaction conditions. As shown in Scheme 1b, 2-benzylidenemalononitrile was obtained successfully in 99% yield at room temperature for 48 h. It is worth mentioning that 50 mg of the catalyst was sufficient in this gram scale reaction, which proved the applicability of this protocol in large scales.

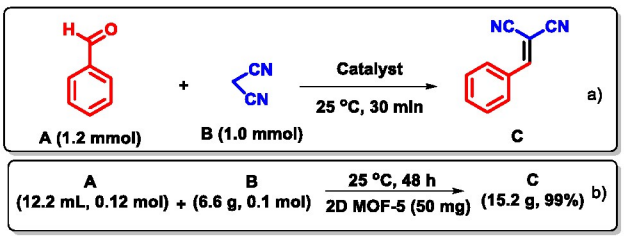

Scheme 1 a) Knoevenagel condensation reaction catalyzed by MOF-5 and other catalysts; b) Gram scale reaction of Knoevenagel condensation catalyzed by 2D MOF-5 nanosheets.

A mechanism for the 2D-MOF-5-catalyzed Knoevenagel condensation reaction of aldehyde and malononitrile was proposed (Scheme 2). The reaction initiates from the

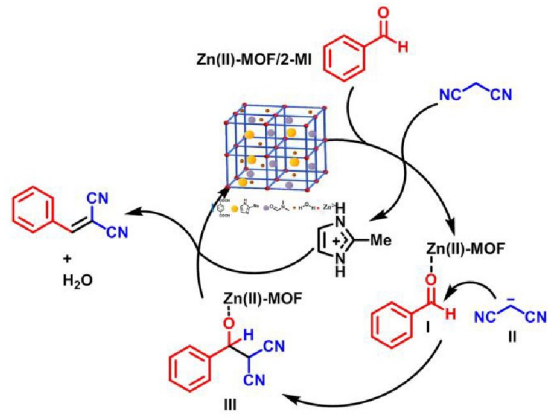

Scheme 2 Proposed catalytic mechanism for Knoevenagel condensation reaction catalyzed by 2D MOF-5.

activation of an aldehyde with the Lewis acid site Zn^{2+} ion center of MOF-5. Uncoordinated 2-MI adsorbed in MOF-5 serves as a base to promote the deprotonation of the active methylene group for the generation of a carbanion intermediate II. Next, the newly formed carbanion II reacts with the activated carbonyl group I on the aromatic aldehyde via nucleophilic attack. Lastly, the addition intermediate III can be quickly converted to the 2-benzylidenemalononitrile product after obtaining one proton and losing water, at the same time with regeneration of the 2D MOF-5 catalyst.

In summary, a novel and facile strategy was developed for the synthesis of 2D MOF-5 catalyst, which employs 2-MI not only as a regulation reagent to control the crystal morphology, but also as a Lewis basic site to form a 2D Zn(II)/2-MI catalyst. The 2-MI can promote deprotonation of carboxylic linkers to accelerate crystal nucleation in the crystal growth process, and also restrict crystal growth along the vertical direction by competitive intercalation with H_2BDC. Multi-technique characterizations revealed that 2-MI may directly exist in the surface or pore of the nanosheet as a guest molecule, or present in the crystal structure of MOF-5 via coordination. While, XRD demonstrated that the existent of 2-MI did not change the crystal structure of MOF-5. The as-prepared nanoplates exhibit much higher catalytic activity than that of bulk MOF-5 for the Knoevenagel condensation reaction of aldehyde and malononitrile under solvent-free and mild conditions. We hope that this strategy will become a useful archetypical template for researchers designing 2D MOFs with unique performance in various fields.

Acknowledgements

This work is supported by the National Natural Science Foundation of China (Grant No. 21502162, 21162027 and 21261022). The Regional Collaborative Innovation Project of Xinjiang Uyghur Autonomous Region (No. 2017E01005), the University scientific research project of Xinjiang Uyghur Autonomous Region (No. XJEDU2017I001).

Conflicts of interest

There are no conflicts to declare.

Notes and references

1 (a) F. Pei, L. Lin, D. Ou, Z. Zheng, S. Mo, X. Fang and N. Zheng, *Nat. Commun.*, 2017, **8**, 482; (b) Q. Lu, Y. Yu, Q. Ma, B. Chen and H. Zhang, Adv. Mater. *Adv. Mater.*, 2016, **28**, 1917-1933.
2 X. Liu, T. Ma, N. Pinna and J. Zhang, *Adv. Funct. Mater.*, 2017, **27**, 1702168-n/a.
3 L. Dai, *Acc. Chem. Res.*, 2013, **46**, 31-42.
4 Y. Chen, C. Tan, H. Zhang and L. Wang, *Chem. Soc. Rev.*, 2015, **44**, 2681-2701.
5 (a) M. Zhao, Q. Lu, Q. Ma and H. Zhang, *Small Methods,* 2017, **1**, 1600030-n/a; (b) A. J. Clough, J. W. Yoo, M. H. Mecklenburg and S. C. Marinescu, *J. Am. Chem. Soc.*, 2015, **137**, 118-121; (c) G. Zhan and H. C. Zeng, *Adv. Funct. Mater.*, 2016, **26**, 3268-3281.
6 R. Kumar, K. Jayaramulu, T. K. Maji and C. N. R. Rao, *Dalton,* 2014, **43**, 7383-7386.

View Article Online
DOI: 10.1039/C8CE00954F

7 T. Rodenas, I. Luz, G. Prieto, B. Seoane, H. Miro, A. Corma, F. Kapteijn, F. X. Llabrés i Xamena and J. Gascon, *Nat. Mater.,* 2014, **14**, 48-55.

8 H. Xu, J. Gao, X. Qian, J. Wang, H. He, Y. Cui, Y. Yang, Z. Wang and G. Qian, *J. Mater. Chem A.,* 2016, **4**, 10900-11905.

9 (a) J. Liang, X.-S. Wang and R. Cao, *Chem. Soc. Rev.*, 2017, **46**, 126-157; (b) Y.-B. Huang, Q. Wang, J. Liang, X. Wang and Rong Cao, *J. Am. Chem. Soc.*, 2016, **138**, 10104-10107; (c) J. Liang, R.-P. Chen, X.-Y. Wang, T.-T. Liu, X.-S. Wang, Y.-B. Huang and R. Cao, *Chem. Sci.*, 2017, **8**, 1570-1575.

10 (a) Y. Peng, Y. Li, Y. Ban, H. Jin, W. Jiao, X. Liu and W. Yang, *Science,* 2014, **346**, 1356-1359; (b) P.-Z. Li, Y. Maeda and Q. Xu, *Chem. Commun.,* 2011, **47**, 8436-8438.

11 S. Motoyama, R. Makiura, O. Sakata and H. Kitagawa, *J. Am. Chem. Soc.,* 2011, **133**, 5640-5643.

12 (a) Y. Hu, X. Dong, J. Nan, W. Jin, X. Ren, N. Xua and Y. Moo Lee, *Chem. Commun*., 2011,**47**, 737-739; (b) V. V. Guerrero, Y. Yoo, M. C. McCarthy and H.-K. Jeong, *J. Mater. Chem*., 2010, **20**, 3938-3943; (c) D. Kim and A. Coskun, *CrystEngComm*, 2016,**18**, 4013-4017.

13 (a) Y. Wang, M. Zhao, J. Ping, B. Chen, X. Cao, Y. Huang, C. Tan, Q. Ma, S. Wu, Y. Yu, Q. Lu, J. Chen, W. Zhao, Y. Ying and H. Zhang, *Adv. Mater.,* 2016, **28**, 4149-4155; (b) E.-Y. Choi, C. A. Wray, C. Hu and W. Choe, *CrystEngComm,* 2009, **11**, 553-555.

14 M. Xu, S. Yuan, X.-Y. Chen, Y.-J. Chang, G. Day, Z.-Y. Gu and H.-C. Zhou, *J. Am. Chem. Soc.,* 2017, **139**, 8312-8319.

15 H. Li, M. Eddaoudi, M. O'Keeffe and O. M. Yaghi, *Nature,* 1999, **402**, 276-279.

16 S. Turner, O. I. Lebedev, F. Schröder, D. Esken, R. A. Fischer and G. V. Tendeloo, *Chem. Mater.,* 2008, **20**, 5622-5627.

17 J. Hafizovic, M. Bjørgen, U. Olsbye, P. D. C. Dietzel, S. Bordiga, C. Prestipino, C. Lamberti and K. P. Lillerud, *J. Am. Chem. Soc.,* 2007, **129**, 3612-3620.

18 (a) N. Ding, H. Li, X. Feng, Q. Wang, S. Wang, L. Ma, J. Zhou and B. Wang, *J. Am. Chem. Soc.,* 2016, **138**, 10100-10103; (b) L. Bellarosa, C. K. Brozek, M. García-Melchor, M. Dincă and N. López, *Chem. Mater.,* 2015, **27**, 3422-3429; (c) D. Lv, Y. Chen, Y. Li, R. Shi, H. Wu, X. Sun, J. Xiao, H. Xi, Q. Xia and Z. Li, *Chem. Eng. Data,* 2017, **62**, 2030-2036.

19 C. Guo, Y. Zhang, Y. Guo, L. Zhang, Y. Zhang and J. Wang, *Chem. Commun.,* 2018, **54**, 252-255.

20 (a) C. Guo, Y. Zhang, Y. Zhang and J. Wang, *Chem. Commun.,* 2018, **54**, 3701-3704; (b) C. Guo, Y. Zhang, X. Nan, C. Feng, Y. Guo and J. Wang, *Mol. Catal.,* 2017, **440**, 168-174.

21 F. Cao, M. Zhao, Y. Yu, B. Chen, Y. Huang, J. Yang, X. Cao, Q. Lu, X. Zhang, Z. Zhang, C. Tan and H. Zhang, *J. Am. Chem. Soc*., 2016, **138**, 6924-6927.

22 (a) C. Zheng, H. F. Greer, C.-Y. Chiang and W. Zhou, *CrystEngComm,* 2014, **16**, 1064-1070; (b) P. Cubillas, M. W.Anderson and M. P. Attfield, *Chem.–Eur. J.,* 2012, **18**, 15406-15415; (c) C. Wiktor, S. Turner, D. Zacher, R. A. Fischer and G. V. Tendeloo, *Micropor. Mesopor. Mat.,* **2012**, *162*, 131-135.

23 H. Li, W. Shi, K. Zhao, H. Li, Y. Bing and P. Cheng, *Inorg. Chem.,* 2012, **51**, 9200-9207.

24 (a) X.-S. Wang, J. Liang, L. Li, Z.-J. Lin, P. P. Bag, S.-Y. Gao, Y.-B. Huang and R. Cao, *Inorg. Chem.,* 2016, **55**, 2641-2649; (b) F. Martínez, G. Orcajo, D. Briones, P. Leo and G. Calleja, *Micropor. Mesopor. Mat.,* 2017, **246**, 43-50.

25 (a) Y. Luan, Y. Qi, H. Gao, R. S. Andriamitantsoa, N. Zheng and G. Wang, *J. Mater. Chem. A,* 2015, **3**, 17320-17331; (b) S. Zhang, H. He, F. Sun, N. Zhao, J. Du, Q. Pan and Zhu, G. *Inorg. Chem. Commun.,* 2017, **79**, 55-59; (c) D. Wang and Z. Li, *Catal. Sci. Technol.,* 2015, **5,** 1623-1628.

View Article Online
DOI: 10.1039/C8CE00954F

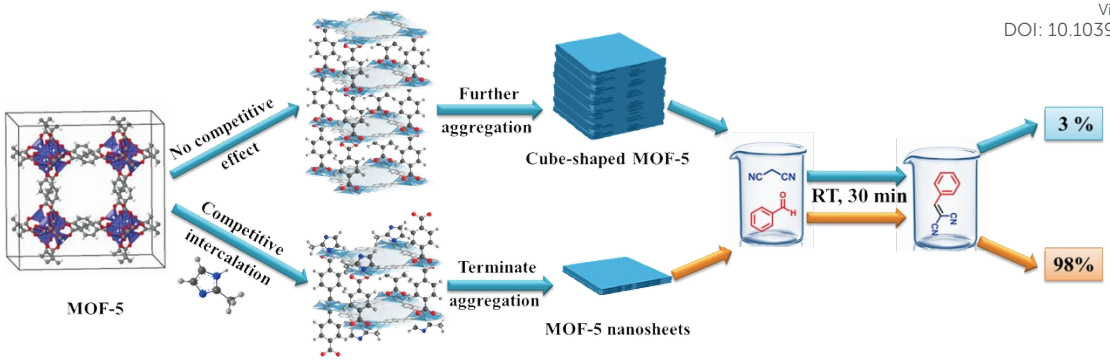

A novel and facile strategy was developed for the synthesis of dual-functionalized 2D MOF-5 catalyst with 2-methyimidazole as a regulation reagents and Lewis basic sites, which showed excellent catalytic activity in Knoevenagel condensation.